Thermal Domain Motions of CheA Kinase in Solution: Disulfide Trapping Reveals the Motional Constraints Leading to Trans-autophosphorylation[†]

Susan L. Gloor and Joseph J. Falke*

Molecular Biophysics Program and the Department of Chemistry and Biochemistry, University of Colorado, Boulder, Colorado 80309-0215

Received January 9, 2009; Revised Manuscript Received March 1, 2009

ABSTRACT: The histidine kinase CheA is a central component of the bacterial chemotaxis signaling cluster, in which transmembrane receptors regulate CheA autokinase activity. CheA is a homodimer, and each of the two identical subunits possesses five different domains with distinct structures and functions. The free enzyme, like the receptor-bound enzyme, catalyzes a trans-autokinase reaction in which the catalytic domain (P4) of one subunit phosphorylates the substrate domain (P1) of the other subunit. Molecular analysis of CheA domain motions has important implications for the mechanism of CheA trans-autophosphorylation, for CheA assembly into the signaling cluster and for receptor regulation of CheA activity. In this initial study of the free CheA dimer, we employ disulfide trapping to analyze collisions between pairs of domains, thereby mapping out the ranges and kinetics of domain motions. A library of 33 functional single-cysteine CheA mutants, all retaining normal autokinase activity, is used to analyze intradimer collisions between symmetric domain pairs. The homodimeric structure of CheA ensures that each mutant contains a pair of symmetric, surface-exposed cysteine residues. Cysteine−cysteine collisions trapped by disulfide bond formation indicate that P1 is the most mobile CheA domain, but large amplitude P2, P4, and P5 domain motions are also detected. The mobility of P1 is further analyzed using a library of 17 functional dicysteine CheA mutants, wherein each mutant subunit possesses one cysteine at a fixed probe position on the P1 domain and a second cysteine on a different domain. The resulting CheA homodimers contain four cysteine residues; thus disulfide trapping yields multiple products that are identified by assignment methods. The findings reveal that the P1 substrate domain collides rapidly with residues on the P4′ catalytic domain in the sister subunit, but no intrasubunit collisions are detected. This observation provides a direct, motional explanation for CheA trans-autophosphorylation, explains why the long linkers of the P1−P2 region do not become tangled in the dimer, and has important implications for other aspects of CheA function. Finally, a working model is proposed for the motional constraints that limit the P1 domain to the region of space near the P4′ catalytic domain of the sister subunit.

The chemotaxis pathways of *Escherichia coli*, *Salmonella typhimurium*, and related bacteria utilize cell-surface receptors to control a cytoplasmic two-component phosphotransfer system, thereby regulating the switching of the flagellar motors between different swimming states (*1*−*6*). The receptors form regular arrays at the cell pole to which the histidine kinase CheA and the coupling protein CheW bind, yielding an ultrastable, ultrasensitive signaling cluster (*7*−*11*). The receptor population regulates the autophosphorylation rate of the bound CheA kinase population, such that the receptor on-state stimulates CheA autophosphorylation and the off-state inhibits it. Following autophosphorylation, as in other two-component signaling pathways, the phosphate moiety of receptor-bound phospho-CheA is transferred from the histidine kinase to the active site of an aspartate kinase. One of the two chemotactic aspartate kinases is CheY, the motor regulator protein, and the other is CheB, an adaptation enzyme. Like receptor-bound CheA, free CheA exhibits autokinase activity and phosphotransfer to CheY or CheB, although the rate of autophosphorylation is much slower in the absence of receptor stimulation.

The CheA protein is a dimer of identical subunits (*12, 13*). Each subunit possesses five structural domains with distinct functions (Figure 1A) (*14*−*16*): (i) The substrate domain, P1, possesses the His48 residue that is phosphorylated by the autokinase reaction, and other active site residues on the same face as His48 (*17, 18*). (ii) The CheY/B binding domain, P2, optimizes phosphotransfer from the P1 domain to CheY or CheB, although this domain is not essential for function (*14, 19, 20*). (iii) The dimerization domain, P3, is a helical hairpin that associates with the symmetric domain of the other subunit to generate a stable four-helix bundle (*21*). (iv) The catalytic domain, P4, possesses the ATP binding site and additional residues that catalyze phosphotransfer from ATP to the P1 domain (*15*). (v) The regulatory domain, P5, binds CheW and the receptor (*22*−*24*). Additional receptor contacts are likely provided by the P3 and P4 domains (*24*).

The five CheA domains are separated by flexible linkers or hinges, suggesting that the relative domain movements could play important roles in the autokinase reaction, in the

[†] Support provided by NIH, Grant NIH R01 GM-040731.

* To whom correspondence should be addressed. E-mail: falke@colorado.edu. Tel: (303) 492-3503. Fax: (303) 492-5894.

10.1021/bi900033r CCC: $40.75 © 2009 American Chemical Society
Published on Web 03/03/2009

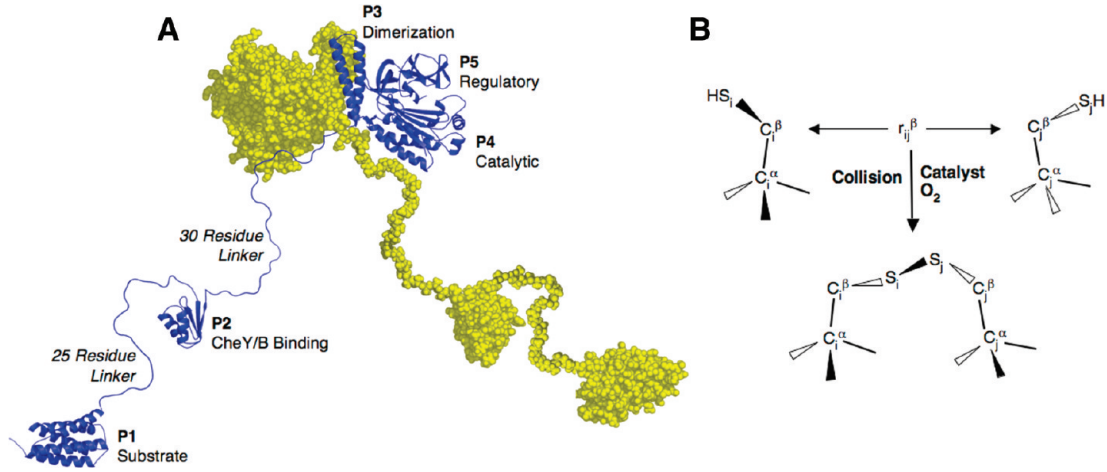

FIGURE 1: The CheA homodimer and the disulfide trapping approach: (A) The present study focuses on the homodimeric histidine kinase CheA of *Salmonella typhimurium*. Shown is a structural model, with one identical subunit in ribbon format (blue) and the other in space filling (gold), pieced together from the high-resolution structures of (i) the P1 substrate domain of *S. typhimurium* CheA (*17*), (ii) the P2 CheY/B binding domain of *E. coli* CheA, which is highly homologous to *S. typhimurium* CheA (*20*), and (iii) the dimeric core region of the homologous *Thermatoga maritima* CheA, containing the P3 dimerization domain, the P4 catalytic domain, and the P5 regulatory domain (*15*). Also shown are simplified models of the long, presumably unstructured P1−P2 and P2−P3 linkers that are 25 and 30 residues in length in *S. typhimurium* CheA, respectively (*17, 20, 22, 23, 25*). Structural evidence indicates that an antiparallel interaction between symmetric β-strands at the N-terminus of the P3 dimerization domain directs the end of the P2−P3 linker toward the sister subunit in the same homodimer, as illustrated (*15*). MacPyMol graphics software (Delano Scientific) was used to build random coil, polyalanine segments of the same length as P1−P2 and P2−P3 and to display all structural elements. (B) Collisions between two cysteine residues can be trapped by oxidative disulfide bond formation. The rate of disulfide formation is defined largely by the collision rate and the efficiency of the oxidation reaction. Local environmental factors, including accessibility to oxidation agent, constraints on collision geometry, and altered sulfhydryl pK_a can also modulate the overall reaction rate (*27*−*32*).

assembly of the receptor−CheA−CheW complex, and in receptor regulation of CheA activity. As illustrated in Figure 1A, the greatest sources of motional freedom are predicted to be the long P1−P2 and P2−P3 linkers, totaling 25 residues (92 Å) and 30 residues (109 Å) in length, respectively (*17, 20, 22, 25*). Assuming these linkers are unstructured, as currently believed, they would confer long-range motional freedom onto the P1 and P2 domains including the ability to contact all surfaces of the dimer. In addition, crystallographic analysis of the P3−P5 core reveals different domain orientations in the two subunits of the dimer, indicating the existence of flexible hinges between those domains (*15*). Finally, the autophosphorylation reaction of CheA occurs via a trans mechanism in which the P4 catalytic domain of one subunit phosphorylates His48 on the P1′ domain of its sister subunit in the same dimer (herein primes are used to distinguish the two subunits), indicating that the P1′ and P4 domains must be able to collide (*12, 13, 26*).

Together these considerations raise interesting questions about the thermal domain dynamics of the CheA dimer: (i) How mobile are the individual domains? (ii) What is the range of motion of the P1 substrate domain relative to the P3−P5 core? (iii) Why is autophosphorylation exclusively trans, and does this trans mechanism arise from constraints on the mobility of the P1 domain, or does the P1 domain exhibit different propensities to be phosphorylated when in the vicinity of the P4 and P4′ domains of different subunits? (iv) How do the P1 and P2 domains of the two subunits, as well as their long P1−P2 and P2−P3 linkers, avoid intertwining and tangling? (v) What are the time scales of domain motions within the CheA dimer?

Such questions can be addressed using an established disulfide trapping approach (*27*−*32*). The approach begins by engineering functional pairs of cysteine residues at selected positions on the surfaces of two different CheA domains. Subsequently, a tunable oxidation reaction is used to trap collisions between those domains as disulfide bonds (Figure 1B). The results reveal that the P1 domain is highly mobile in the vicinity of the P4′ domain of its sister subunit and that P1 is constrained to remain within this region. The constraints on P1 mobility explain why cis-autophosphorylation does not occur and why the P1−P2 regions of the two subunits and their long linkers do not become intertwined and tangled. Other motions of the P1, P2, P4, and P5 domains are also observed and have important implications for CheA function. The rapid domain motions, which are the main focus of the present study, occur on the millisecond time scale or faster.

MATERIALS AND METHODS

Materials. Cysteine-less CheA and single-cysteine mutant CheA proteins were expressed with N-terminal His_6 tags from plasmid pET6H-CheA (constructed from pET28, Novagen; Bornhorst, Munger and Falke, unpublished) in *E. coli* strain BL21(DE3) (Stratagene), then were isolated by standard Ni-NTA affinity chromatography (*24, 33*). His_6-tagged CheY was expressed from plasmid pVSCheY-6H (derived from pVS33, a gift from Victor Sourjik and Howard Berg, Harvard University) in *E. coli* strain M15 containing pREp4 (Qiagen). Protein purity and concentration were determined by Laemmli SDS−PAGE (*34*).

Reagents were obtained from the following sources: [γ-^{32}P]-ATP from Perkin-Elmer; QuickChange site-directed mutagenesis kit from Stratagene; oligonucleotides from Integrated DNA Technologies; restriction enzymes from New England Biolabs; sulfhydryl-specific probe 5-fluorescein-maleimide (5FM) from Molecular Probes Invitrogen; all other reagent grade chemicals from Sigma unless noted otherwise.

Mutagenesis. Site-directed mutagenesis was performed as previously described (*24, 35*) using the PCR-based QuickChange mutagenesis kit to engineer point mutations into *Salmonella typhimurium* cysteine-less CheA in plasmid pET6H-CheA. Silent restriction sites were designed into the mutagenic primers, where possible, allowing screening for cysteine mutants by restriction. All resulting plasmids were sequenced to directly confirm the desired mutations, then CheA mutants were expressed and purified as described above.

Free CheA Autokinase Assay. Free CheA was mixed with CheY to a final concentration of 4 μM CheA and 55 μM CheY in reaction buffer (50 mM Tris, pH 7.5 with HCl, 50 mM KCl, and 5 mM $MgCl_2$). The previously described (*36*) autophosphorylation reaction was started by addition of [γ-^{32}P]-ATP. The concentration of CheY was sufficient to ensure that CheA autophosphorylation was the rate-determining step. After 10 s, the reaction was quenched by the addition of 3 times the reaction volume of 2× Laemmli sample buffer containing 25 mM EDTA. The unheated samples were then loaded onto 15% acrylamide (acrylamide/bisacrylamide 40:1.25), 20% urea (w/v) Laemmli SDS−PAGE gels. The resulting gels were dried and phosphorimaged (Molecular Dynamics) to quantify the level of [γ-^{32}P]-phospho-CheY, which is proportional to the initial rate of CheA autophosphorylation. All reactions were performed in triplicate.

Disulfide Trapping Reactions. Collisions between pairs of CheA cysteine residues were trapped by oxidative disulfide bond formation. Disulfide trapping reactions employed a total concentration of CheA subunits (4 μM) that was 10-fold higher than the dissociation constant for dimerization (K_D = 0.2−0.5 μM (*12, 37*); S. Buehler and J. Falke, unpublished), thereby ensuring that the monomer−dimer equilibrium was driven strongly toward the dimer. The reaction buffer (50 mM Tris, pH 7.5 with HCl, 50 mM KCl, and 5 mM $MgCl_2$) is the same buffer used in kinase assays for free CheA (see above) and for receptor-coupled CheA kinase in the reconstituted signaling cluster (*24*), thereby ensuring that CheA is in a native state during the disulfide trapping reaction. This initial study of apo-CheA is carried out in the absence of its substrate ATP and its binding partners CheR, CheW, and CheY.

Three oxidation strengths were employed to adjust the disulfide formation rates so that they could be easily quantified. All oxidation reactions were carried out at 30 °C at an ambient dissolved O_2 concentration of 200 μM using general methods described previously (*28, 32, 38*). Reactions were initiated by the addition of the redox catalyst Cu(II)(1,10-phenanthroline)$_3$ (or $CuPhen_3$),[1] together with the chelator EDTA, which serves to reduce the oxidation rate by competitively binding Cu(II) ions. The three oxidation reactions were (i) mild, 0.2 mM $CuPhen_3$, 5.0 mM EDTA, 10 s reaction time; (ii) moderate, 0.5 mM $CuPhen_3$, 5.0 mM EDTA, 60 s reaction time; and (iii) strong, 1.0 mM $CuPhen_3$, 0.8 mM EDTA, 300 s reaction time. Reactions were quenched by the addition of an equal volume of 4×-Laemmli SDS−PAGE sample buffer (thereby providing twice the usual SDS to ensure complete solubilization) supplemented with 40 mM EDTA to chelate the Cu(II) and 40 mM *N*-ethylmaleimide to block free sulfhydryls, followed by heating at 95 °C for 2 min. Products were resolved by running the samples on 10% acrylamide (40:1 ratio of acrylamide/bisacrylamide) Laemmli SDS−PAGE gels. Except where noted in the figures, gels were stained with Coomassie blue. The fractional dimer formation was quantified on a per subunit basis [mole dimer × 2/(mole dimer × 2 + mole monomer)] as previously described (*38*) from the intensities of Coomassie-stained bands integrated by ImageJ (NIH).

Distinguishing Intra- And Interdimer Contributions to Covalent Dimer Formation. The contributions of intra- and interdimer collisions to the formation of disulfide-linked CheA dimers were determined from the dependence of the reaction rate on CheA concentration. Oxidation reactions were carried out at 30 °C and quantified as above, except the CheA concentration in the reactions ranged from 2 to 10 μM, and the oxidation strength was tuned, where possible, to ensure that the extent of disulfide formation did not exceed 50%. For a given mutant, the reaction ranged from standard, moderate conditions to a milder oxidation condition: the weakest oxidation was 0.025 mM $CuPhen_3$, 5.0 mM EDTA, 60 s.

Resolving Multiple Products Formed by Dicysteine Mutants. Most of the multiple products generated by disulfide trapping analysis of dicysteine CheA mutants could be identified by their relative migration rates on SDS−PAGE, in comparison with appropriate controls (see Results) (*32, 39*).

Subunit exchange analysis provided a complementary approach that directly assigned asymmetric, single-disulfide products (*39*). Solutions containing either (i) 4 μM CheA single-cysteine mutant X, (ii) 4 μM CheA single-cysteine mutant Y, (iii) 4 μM CheA dicysteine mutant X/Y, or (iv) 2 μM single-cysteine mutant X and 2 μM single-cysteine mutant Y were incubated at 22 °C for 2 h to ensure significant exchange of subunits between dimers prior to oxidation (*21*). Products of the oxidation reaction were visualized on 12.5% acrylamide (acrylamide/bisacrylamide 40:1) Laemmli SDS−PAGE gels and quantified as above.

Kinetic analysis provided a third complementary approach and was particularly useful in the assignment of asymmetric, double-disulfide products (*38*). To drive oxidation to different extents of disulfide bond formation, reactions were carried out under all three conditions (mild, moderate, and strong oxidation) described above. Samples were quenched by mixing with an equal volume of 4× Laemmli sample buffer containing 40 mM EDTA and 1 mM 5-fluorescein-maleimide (5FM) and incubating at 95 °C for 1 min, followed by another incubation in the dark at 22 °C for 10 min. Products were run on 10% acrylamide (acrylamide/bisacrylamide 40:1) Laemmli SDS−PAGE gels. The gels were first imaged on a UV transilluminator using a 470 nm long-pass filter to visualize 5FM fluorescence, then stained with Coomassie blue and imaged as usual. The 5FM reacts specifically with free sulfhydryls, thereby directly identifying products that contain free cysteine residues.

[1] Abbreviations: $CuPhen_3$, Cu(II)(1,10-phenanthroline)$_3$; 5FM, 5-fluorescein maleimide; NEM, *N*-ethyl maleimide; DTT, dithiothreitol; EDTA, ethylene diamine tetraacetic acid.

RESULTS

Strategy. To analyze the thermal domain motions of CheA in solution, the present study uses disulfide trapping to detect interdomain collisions (*27*−*32*). The disulfide trapping method begins by introducing pairs of engineered cysteine residues at defined locations on the protein surface. Typically, these surface cysteine residues are nonperturbing due to the small size and chemical adaptability of the cysteine side chain and its sulfhydryl moeity, which becomes a partially charged sulfanion in polar surroundings or a hydrophobic, fully protonated sulfhydryl in apolar surroundings. Subsequently, intramolecular collisions between pairs of cysteine residues are trapped and detected via oxidative disulfide bond formation. In a protein of known structure, the cysteine pairs that collide reveal the spatial range of the thermal backbone fluctuations underlying collisions (Figure 1B). Finally, where possible, the kinetics of disulfide formation are quantified using a tunable oxidation system. For surface cysteine residues, the sulfhydryl−sulfhydryl collision rate plays the dominant role in defining the disulfide formation rate, although local environmental and steric factors can also play a role (reviewed in ref *32*). Thus, the disulfide trapping method provides insights into both the spatial amplitudes and kinetics of domain motions.

This initial study of domain motions in the CheA dimer focused on the apo protein, in the absence of substrate ATP and protein binding partners (receptor, CheW, CheY, CheR). The disulfide trapping analysis employed a library of previously constructed, engineered cysteine residues (*24*) at selected surface positions on the five CheA domains as summarized in Table 1 and Figure 2. A cysteine-less CheA protein, previously engineered to remove all three intrinsic cysteine residues while retaining normal kinase activity and regulation (*24*), was used as the background for the introduction of mutant cysteine residues. Since CheA is a homodimer, each single cysteine substitution yielded a dimer possessing two cysteine residues at symmetric subunit positions (Figure 2A). Single-cysteine mutants that retained kinase function were used to probe for collisions between symmetric domains within the same CheA dimer via disulfide trapping. In parallel, a second library of dicysteine mutants was created, with one cysteine residue at a constant probe position on the P1 substrate domain, and a second cysteine residue located on a different domain. Such dicysteine mutants form homodimers with two symmetric pairs of cysteine residues (Figure 2A). Di-cysteine mutants that retained kinase function were used to analyze collisions between P1 and other domains in the CheA dimer via disulfide trapping.

Figure 2A summarizes the five different types of collisional mechanisms that can produce disulfide bond formation in the CheA dimer system. To resolve the type of collision underlying the formation of a given disulfide-containing product, mechanistic analysis was carried out to ascertain whether a detected collision occurred between cysteine residues in the same dimer (intradimer) or in different dimers (interdimer) (*32*) (Figure 2A). For intradimer collisions in dicysteine mutants, additional mechanistic studies determined whether the collision involves two cysteine residues in the same subunit (intrasubunit) or different subunits (intersubunit) (Figure 2A) and whether the collision was between symmetric or asymmetric domains within the dimer (Figure 2A). In cases where multiple products were formed, assignment studies were carried out to identify the number and types of disulfide bonds within each product. Finally, the spatial ranges of the disulfide-trapped collisions were analyzed to map out the amplitudes of domain motions, while the disulfide formation rates were employed to establish lower limits on the collision frequencies.

Table 1: Single-Cysteine CheA Mutants and Properties

mutant	domain, function	kinase activity (rel)[a]	S−S formation rate (rel)[b]	fraction (%) intradimer[c]
cysteine-less		1.0 ± 0.1	*d*	*d*
Q10C	P1, substrate	1.4 ± 0.1	rapid	100 ± 10
D17C	P1, substrate	1.4 ± 0.1	slow	*e*
Q25C	P1, substrate	1.1 ± 0.1	slow	*e*
A37C	P1, substrate	1.6 ± 0.1	intermediate	46 ± 5
T60C	P1, substrate	1.1 ± 0.1	slow	*e*
E75C	P1, substrate	1.1 ± 0.1	slow	*e*
Q82C	P1, substrate	1.0 ± 0.1	slow	*e*
E93C	P1, substrate	1.3 ± 0.1	slow	*e*
E109C	P1, substrate	1.1 ± 0.1	rapid	82 ± 8
A114C	P1, substrate	1.5 ± 0.1	rapid	84 ± 8
Q125C	P1, substrate	1.0 ± 0.1	rapid	81 ± 8
R171C	P2, CheY/B binding	1.3 ± 0.1	rapid	100 ± 10
D192C	P2, CheY/B binding	0.9 ± 0.1	slow	*e*
V216C	P2, CheY/B binding	0.8 ± 0.1	slow	*e*
K230C	P2, CheY/B binding	0.8 ± 0.1	slow	*e*
E311C	P3, dimerization	1.0 ± 0.1	intermediate	93 ± 9
S340C	P3, dimerization	0.9 ± 0.1	slow	*e*
S351C	P4, catalytic	1.1 ± 0.1	slow	*e*
D359C	P4, catalytic	0.4 ± 0.1	slow	*e*
E369C	P4, catalytic	1.4 ± 0.1	slow	*e*
I388C	P4, catalytic	0.3 ± 0.1	*e*	*e*
H401C	P4, catalytic	0.0 ± 0.1	*e*	*e*
E425C	P4, catalytic	0.7 ± 0.1	slow	*e*
Q454C	P4, catalytic	0.6 ± 0.1	slow	*e*
E460C	P4, catalytic	0.8 ± 0.1	rapid	80 ± 8
M469C	P4, catalytic	0.7 ± 0.1	rapid	72 ± 7
S514C	P4, catalytic	0.7 ± 0.1	intermediate	50 ± 5
L521C	P4, catalytic	0.7 ± 0.1	slow	*e*
E539C	P5, regulatory	0.7 ± 0.1	slow	*e*
L545C	P5, regulatory	0.5 ± 0.1	slow	*e*
E570C	P5, regulatory	1.2 ± 0.2	slow	*e*
Q596C	P5, regulatory	0.7 ± 0.1	intermediate	100 ± 10
R607C	P5, regulatory	0.9 ± 0.1	rapid	100 ± 10
L627C	P5, regulatory	1.1 ± 0.1	intermediate	100 ± 10
G636C	P5, regulatory	0.7 ± 0.1	intermediate	83 ± 8

[a] Autokinase activity of indicated homodimer, relative to cysteine-less. Activities <0.4 not pursued further. [b] Relative rate of disulfide-linked dimer formation, as defined in Figure 3C, moderate conditions. Slow rates not pursued further. [c] Fraction of covalent dimers formed by intradimer mechanism, as determined in Figure 4B. Fractions <80% not pursued further. [d] Not applicable. [e] Not determined.

A Functional Single-Cysteine Mutant Library for the Analysis of Symmetric Domain Collisions. A set of 35 previously constructed, single-cysteine CheA mutants (*24*) was used as a starting point to develop a library of functional single-cysteine mutants. The 35 cysteine positions were scattered across the surfaces of all five CheA domains (Figure 2B, Table 1). Each single-cysteine mutant was purified in its reduced form, and its autokinase activity was tested in a standard assay (Materials and Methods). Altogether, 33 of the mutants retained at least 40% of the cysteine-less kinase activity and were operationally defined as functional. The remaining two mutants (I388C, H401C) exhibited lower kinase activities (Table 1) and possessed the cysteine residues closest to the ATP binding site. These two mutants were discarded.

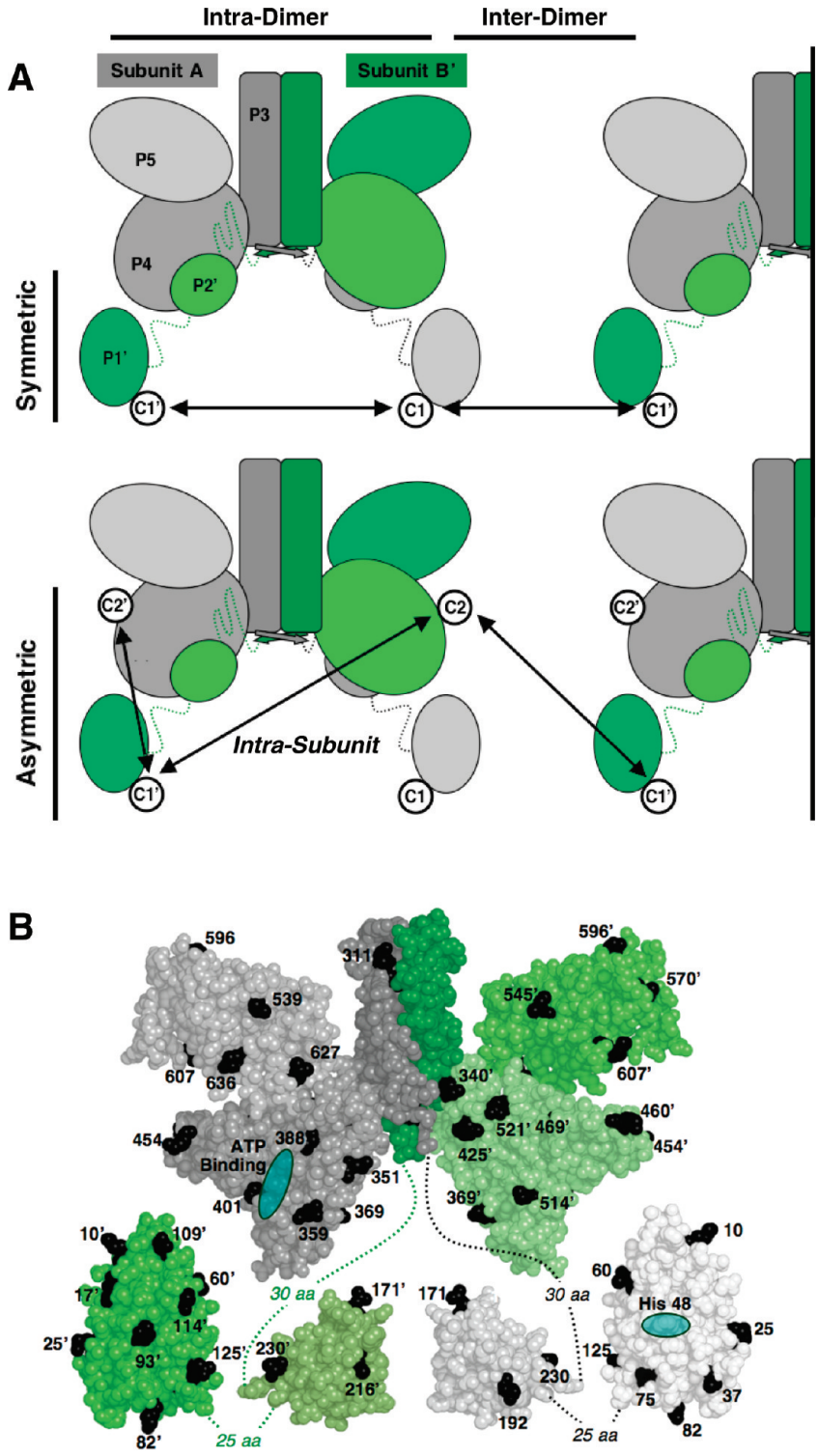

FIGURE 2: Five relevant types of cysteine−cysteine collisions and the starting library of surface cysteine substitutions: (A) Both single-cysteine (upper) and dicysteine (lower) mutants of CheA are employed in the present disulfide trapping study of domain motions. These mutants form CheA homodimers containing one or two pairs of symmetric cysteine residues (C*n*), respectively. One subunit of the homodimer is shown in shades of gray, the other in shades of green. Residues of the two subunits are distinguished by a prime. In single-cysteine mutants, collisions may be detected between the symmetric pairs of cysteine residues on identical domains, and these intersubunit collisions can occur within the same dimer (intradimer) or between dimers (interdimer). In dicysteine mutants, the same types of symmetric collisions may be detected, as well as intra- and interdimer asymmetric collisions between cysteine pairs on different types of domains. In addition to intersubunit collisions, dicysteine mutants can, in principle, also exhibit asymmetric collisions between the two cysteine residues in the same subunit (intrasubunit). (B) Starting library of 35 surface cysteine mutations engineered into a cysteine-less CheA background for disulfide trapping studies (*24*). Again, the two subunits are distinguished by color (gray, green) and by a prime. Also shown are the locations of the His48 phosphorylation residue on the P1 substrate domain and the ATP binding site on the P4 catalytic domain (ovals). In the autophosphosphorylation reaction, known to be trans, the P4 catalytic domain of one domain phosphorylates His48′ on the P1′ substrate domain of the other subunit (*12, 13, 26*).

Identification of Symmetric Cysteine Pairs That Form Disulfide Bonds. To analyze symmetric domain collisions in the apo CheA protein, each mutant homodimer possessing a pair of symmetric cysteine residues at identical positions

in the two subunits was prepared in the standard reaction buffer utilized for kinase activity measurements (50 mM Tris, pH 7.5 with HCl, 50 mM KCl, 5 mM $MgCl_2$) in the absence of substrate ATP. The dissolved, ambient O_2 concentration was 200 μM, but no sulfhydryl oxidation occurred until the addition of the redox catalyst Cu(II)(1,10-phenanthroline)$_3$. In the presence of catalyst, collisions between sulfhydryls were trapped by oxidative disulfide bond formation until the oxidation reaction was quenched at the desired end point. Reaction products were analyzed by SDS−PAGE, yielding resolution of slowly migrating, covalent dimers from the rapidly migrating, individual subunits of noncovalent dimers dissociated by SDS.

As previously observed for other proteins (*32, 39*), the dimer migration rate on SDS−PAGE was a function of the location of the disulfide bond cross-linking the two polypeptide chains (Figure 3A). Thus, when the cross-link was located near the ends of two unfolded chains the average conformation of the covalent dimer was nearly linear. The resulting dimer was able to snake through the gel matrix with less friction, yielding a faster migration rate than when the cross-link was located near the middles of the unfolded chains, yielding a more X-shaped conformation that generated more friction and slowed migration in the gel. As expected, the covalent disulfide linkages were fully reversed by treatment with reducing agent (Figure 3B).

Three different oxidation strengths, mild, moderate and strong, were tested to tune the kinetics of disulfide bond formation for the present cysteine mutant library (*32*). These three oxidation strengths all utilized a reaction temperature of 30 °C, the optimal temperature for chemotaxis (*40, 41*), but differed in (i) the concentration of redox catalyst (0.2, 0.5, and 1.0 mM, respectively), (ii) the concentration of EDTA used to buffer the catalytic Cu(II) ion (5.0, 5.0, and 0.8 mM, respectively), and (iii) the length of the oxidation reaction (10, 60, and 300 s, respectively). Increasing the oxidation strength generated higher levels of disulfide bond formation, as expected (Figure 3C). The moderate oxidation strength was chosen as the standard condition because it yielded, for most of the 33 cysteine positions, easily quantified levels of disulfide bond formation without leaving the initial, linear phase of the reaction (Figure 3C). This moderate oxidation strength was used to operationally define the disulfide formation rate as slow, intermediate, or rapid for each pair of symmetric cysteine residues, yielding 8 rapid pairs, 6 intermediate pairs, and 19 slow pairs (Figure 3C and Table 1).

Analysis of Symmetric Disulfide Reactions To Resolve Intra- and Interdimer Collisions. Two different mechanisms, involving intra- or interdimer collisions, could generate the symmetric disulfide bond products observed in any given reaction (Figure 2A). To resolve these intra- and interdimer contributions, the dependence of the disulfide formation rate on the concentration of protein was determined for the 14 symmetric cysteine pairs exhibiting rapid or intermediate disulfide formation rates. For each rapid reaction where the standard, moderate oxidation conditions pushed the extent of disulfide formation toward completion, a customized, milder oxidation condition was developed to prevent the reaction from exceeding 50% dimer formation, thereby enabling the reaction to remain within its initial, approximately linear phase during the mechanistic test. One reaction (A114C) was so fast that even the mildest oxidation conditions yielded disulfide formation extents over 50%.

For intradimer reactions, the fraction of CheA converted to disulfide-linked dimer was independent of the CheA concentration (Figure 4A, left), while for interdimer reactions higher CheA concentrations yielded higher fractions of disulfide-linked dimer (Figure 4A, right). Some reactions exhibited contributions from both intra- and interdimer mechanisms that could be resolved by plotting the extent of dimer formation versus CheA concentration (Figure 4B). For a given reaction, the contribution from the intradimer mechanism was determined by extrapolating the fraction of disulfide-linked dimer observed at the standard CheA concentration (4 μM) to the fraction observed at zero concentration, where the interdimer mechanism vanishes. Since CheA is a dimer at all concentrations tested, the extrapolation to zero concentration conveniently eliminates any contribution due to dimer dissociation that would be observed in a real experiment at very low CheA concentration.

Table 1 summarizes the contributions of the intra- and interdimer mechanisms to each of the 14 rapid and intermediate disulfide formation reactions. Altogether, 11 of these reactions were dominated (≥80%) by the intradimer mechanism, while the remaining three reactions yielded large contributions (28−54%) from the interdimer mechanism. Of the seven most rapid, intradimer reactions, four were P1−P1′ collisions (or 36% of the P1 positions tested), one was a P2−P2′ collision (25% of the P2 positions tested), one was a P4−P4′ collision (9% of the P4 positions tested), and one was a P5−P5′ collision (14% of the P5 positions tested). Thus, the P1 substrate domain exhibited the highest propensity toward collisions with its symmetric counterpart in the same CheA dimer, confirming that this domain is mobile as expected for its location at the end of a flexible tether.

Functional Dicysteine CheA Mutants To Detect Asymmetric Domain Collisions. To analyze the spatial and kinetic range of the mobile P1 substrate domain, a library of 17 dicysteine mutants was created to probe for asymmetric collisions between P1 and other domains of the CheA dimer. Of particular interest were P1 collisions with three domains of the CheA core: the P3 dimerization domain, the P4 catalytic domain, and the P5 regulatory domain. Together, these P1 substrate and P3−P5 core domains are sufficient for CheA kinase activity *in vitro* and for CheA function *in vivo* (*14, 19*). The cysteine substitution Q10C on the P1 domain was chosen as a constant probe position, because the corresponding single-cysteine mutant retained kinase activity and exhibited purely intradimer disulfide bond formation with no detectable tendency to form interdimer disulfides (Figure 3, Table 2). The 17 positions selected for a second cysteine substitution were scattered over the surfaces of the core domains and retained kinase activities as single-cysteine mutants (Table 2, Figure 2B). Thus, each of the 17 dicysteine pairs included both (i) the probe cysteine residue at the Q10C position and (ii) a second cysteine residue on the P3, P4, or P5 domain in the same CheA subunit. All 17 pairs were found to retain CheA kinase activity (≥50% of the cysteine-less activity, Table 2) and thus were subjected to disulfide trapping analysis.

Identification of Asymmetric Cysteine Pairs That Form Disulfide Bonds. To analyze asymmetric domain collisions in apo-CheA, each dicysteine mutant was prepared in

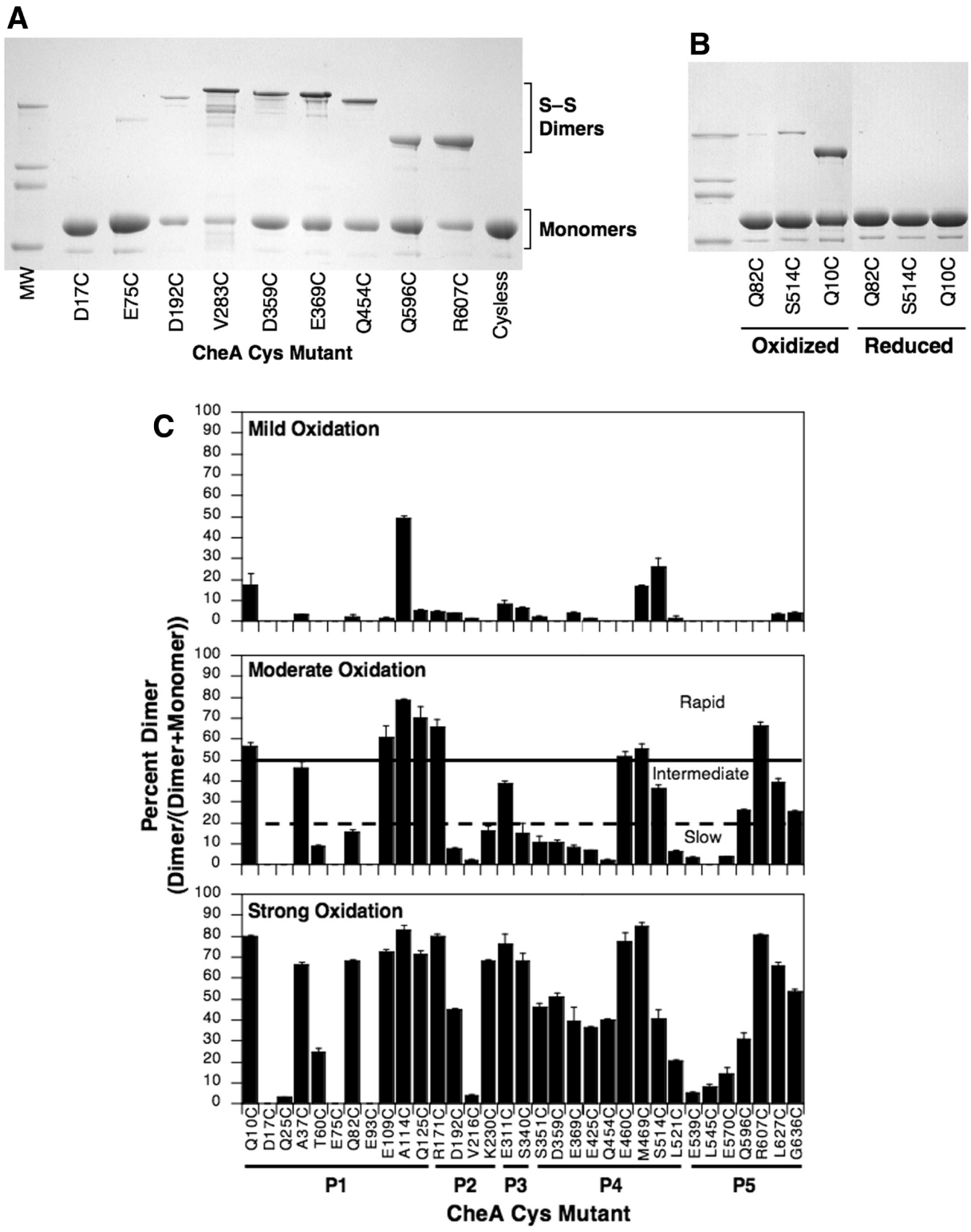

FIGURE 3: Disulfide trapping analysis of symmetric domain−domain collisions. (A) SDS−PAGE analysis of oxidation reactions for representative single-cysteine CheA mutants. In these reactions, the CheA homodimer possesses two symmetric cysteine residues, one on each subunit. Oxidation yields covalent, disulfide-linked dimers (upper band) as well as un-cross-linked subunits that are monomeric following dissociation in SDS (lower band). The dimer migration rate is sensitive to the location of the cross-link: the slowest migration is exhibited by dimers containing a disulfide bond near the middle of the two polypeptide chains (*27, 31, 32, 39*). (B) Reduction of three representative disulfide-linked dimers to monomers by 40 mM DTT in the Laemmli sample buffer confirms that the covalent cross-link is reversible. (C) Extents of disulfide-linked dimer formation for the 33 functional single-cysteine CheA mutants exposed to three different oxidation strengths. The moderate oxidation strength was used as the standard condition, and the horizontal lines delineate the operational definitions of slow (below the dashed line), intermediate (between the two lines), and rapid (above the upper, solid line) disulfide formation reactions. Fractional disulfide formation (dimer/(dimer + monomer)) is calculated on a per subunit basis (mole dimer × 2/(mole dimer × 2 + mole monomer)). Reaction conditions, all at 30 °C in reaction buffer (50 mM Tris, pH 7.5 with HCl, 50 mM KCl, 5 mM $MgCl_2$): (i) mild oxidation = 4 μM CheA, 0.2 mM $CuPhen_3$, 5.0 mM EDTA, 10 s; (ii) moderate oxidation = 4 μM CheA, 0.5 mM $CuPhen_3$, 5.0 mM EDTA, 60 s; (iii) strong oxidation = 4 μM CheA, 1.0 mM $CuPhen_3$, 0.8 mM EDTA, 300 s.

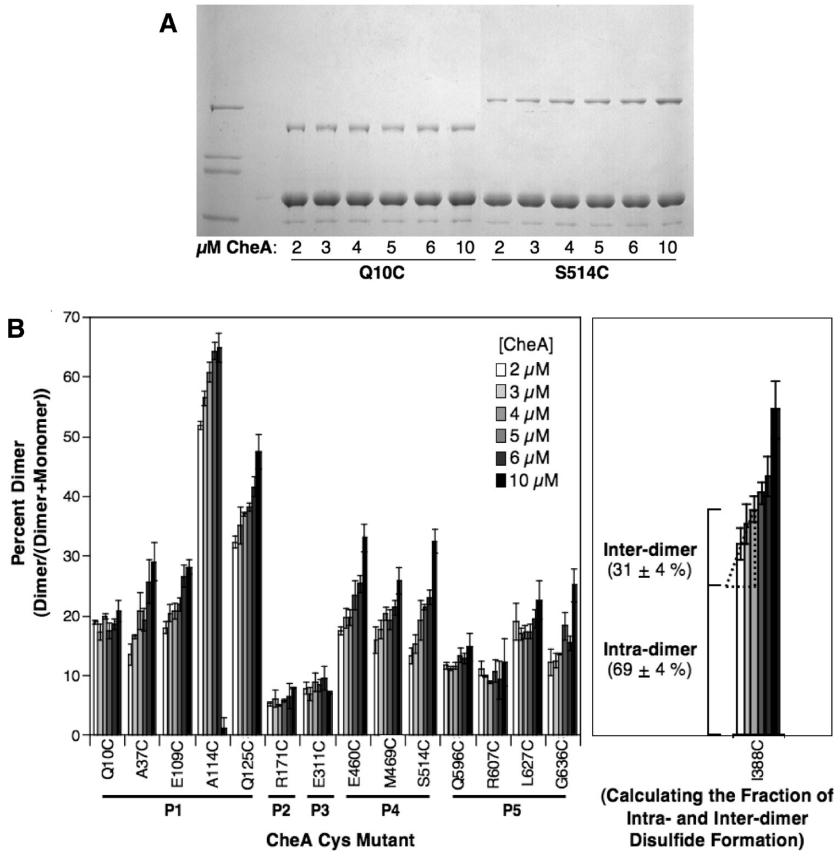

FIGURE 4: Resolution of intra- versus interdimer mechanisms for symmetric domain−domain collisions. (A) Oxidative disulfide reactions were carried out at the indicated CheA concentrations; then the quenched reactions were diluted to give the same amount of total CheA in each lane on SDS−PAGE. For purely intradimer disulfide reactions, the fractional disulfide formation is independent of the CheA concentration as exemplified by Q10C. For interdimer disulfide reactions, the fractional disulfide formation increases rapidly with increasing CheA concentration as exemplified by S514C. (B) CheA concentration dependence of oxidative disulfide bond formation for the 14 single-cysteine mutants that form disulfide-linked dimers at intermediate or rapid rates (Figure 3C and Table 1). Reactions with large contributions from interdimer reactions are dependent on CheA concentration. An extrapolation method was used to resolve the contributions of intra- and interdimer collisions to disulfide formation, as illustrated for a representative mutant (right). This method extrapolates (dashed line) the disulfide formation extents measured for CheA concentrations of 4 μM (the concentration used in standard oxidative reactions), 3 μM, and 2 μM to an imaginary CheA concentration of 0 μM, where the contribution of interdimer collisions becomes negligible. Since CheA is predominantly dimeric at all concentrations tested (see text), the extrapolation conveniently removes the effect of dimer dissociation that would be observed in a real reaction at vanishingly low CheA concentration. Oxidation conditions were tuned, where possible, to ensure that the extent of disulfide formation did not exceed 50%. For a given mutant, the oxidation reaction at 30 °C ranged from the standard, intermediate condition (see Figure 3 legend) to a milder condition, where the weakest condition utilized was 4 μM CheA, 0.025 mM $CuPhen_3$, 5.0 mM EDTA, 60 s.

standard reaction buffer in the absence of ATP (same buffer as that used in the single-cysteine studies). Each of the identical subunits in the resulting homodimer possessed two cysteine residues at the same two positions, such that each dimer contained four cysteine residues arranged in two symmetric pairs (Figure 2A). In principle, a given cysteine residue could form three different types of disulfide bonds (Figure 2A): (i) the intrasubunit, asymmetric disulfide X−Y formed between the two cysteine residues in the same subunit, (ii) the intersubunit, asymmetric disulfide X−Y′ formed between cysteine residues at different positions in separate subunits, and (iii) the intersubunit, symmetric disulfide X−X′ or Y−Y′ formed between two cysteine residues at the same positions in different subunits. Furthermore, a covalent dimer can be linked by either one disulfide (X−X′ or Y−Y′ or X−Y′) or by two disulfides (symmetric X−X′ and Y−Y′ or asymmetric X−Y′ and X′−Y). Finally, a covalent dimer can be formed via an intradimer or interdimer collisional mechanism (Figure 2A). The various disulfide-containing products were readily resolved and assigned by SDS−PAGE migration analysis and other methods (*27*−*32, 38, 39*), as illustrated in Figure 5A and detailed further below.

The 17 dicysteine mutants were subjected to the same mild, moderate, and strong oxidation conditions described for the single-cysteine mutants. CheA is capable of forming intrasubunit disulfide bonds, as illustrated by the intrasubunit disulfide product rapidly formed by a positive control dicysteine mutant D359C/Q596C possessing cysteine residues on the P4 and P5 domains (Figure 5A, left panel). Such intrasubunit disulfides make the polypeptide chain more compact, so it migrates faster than the reduced monomer on SDS−PAGE as observed for D359C/Q596C (*28, 32, 39*). The spacing between the two cysteine residues in all 17 dicysteine mutants (Table 2) is greater than the spacing in D359C/Q596C; thus each intrasubunit disulfide would be easily detected by its faster SDS−PAGE migration if formed. Strikingly, however, none of the 17 dicysteine mutants yielded rapidly migrating intrasubunit disulfide products. (A minor band migrating faster than the CheA monomer was observed for all CheA preparations including cysteine-less CheA in the gels of Figures 3 and 5; this band was CheA-

Table 2: Properties of Double-Cysteine CheA Mutants

mutant	domains	kinase activity (rel)[a]	S−S formation rate (rel)[b]	major S−S type[c]	fraction (%) intradimer[d]
cysteine-less		1.0 ± 0.1	*e*	*e*	*e*
Q10C−E311C	P1−P3	1.4 ± 0.2	rapid	asym	87 ± 9
Q10C−S351C	P1−P4	0.9 ± 0.1	rapid	asym	100 ± 10
Q10C−D359C	P1−P4	0.5 ± 0.1	rapid	asym	86 ± 9
Q10C−E369C	P1−P4	0.9 ± 0.1	rapid	asym	81 ± 8
Q10C−E425C	P1−P4	1.3 ± 0.1	rapid	asym	100 ± 10
Q10C−Q454C	P1−P4	1.1 ± 0.1	rapid	asym	100 ± 10
Q10C−E460C	P1−P4	1.6 ± 0.2	rapid	asym	91 ± 9
Q10C−M469C	P1−P4	1.6 ± 0.2	rapid	asym	100 ± 10
Q10C−S514C	P1−P4	1.6 ± 0.1	rapid	asym	49 ± 5
Q10C−L521C	P1−P4	1.7 ± 0.1	intermediate	*f*	*f*
Q10C−E539C	P1−P5	1.3 ± 0.1	intermediate	*f*	*f*
Q10C−L545C	P1−P5	1.6 ± 0.1	intermediate	*f*	*f*
Q10C−E570C	P1−P5	1.5 ± 0.2	intermediate	*f*	*f*
Q10C−Q596C	P1−P5	1.0 ± 0.2	intermediate	*f*	*f*
Q10C−R607C	P1−P5	1.6 ± 0.3	rapid	sym	*f*
Q10C−L627C	P1−P5	1.8 ± 0.2	rapid	sym	*f*
Q10C−G636C	P1−P5	1.2 ± 0.1	intermediate	*f*	*f*

[a] Autokinase activity of indicated homodimer, relative to cysteine-less. Activities <0.4 not pursued further. [b] Relative rate of disulfide-linked dimer formation, as defined in Figure 3C, mild conditions. Slow or intermediate rates not pursued further. [c] Major (>80%) type of intersubunit disulfide bond observed in assignment studies: symmetric (X−X′) or asymmetric (X−Y′). Symmetric disulfides not pursued further. [d] Fraction of covalent dimers formed by intradimer mechanism, as determined in Figure 4B. Fractions <80% not pursued further. [e] Not applicable. [f] Not determined.

short, a truncated version formed by an alternative translation start site within the P1 domain, and is not an intrasubunit disulfide product. Minor disulfide-linked dimer products observed in some reactions are also attributed to CheA homodimers or heterodimers containing CheA-short).

While the 17 dicysteine mutants yielded no detectable intrasubunit disulfide bonds, all rapidly formed intersubunit disulfide bonds under moderate oxidation conditions, yielding covalent dimers. These reactions were so fast that most approached completion and went beyond the initial, linear range of the reaction (data not shown). Thus, to maximize the number of reactions in the linear range, the mild oxidation condition was used for dicysteine mutants. Even under these mild conditions, 11 of the mutants formed disulfide-linked dimers rapidly, while the remaining six mutants formed dimers at intermediate rates (Table 2).

Overall, these findings indicate that the probe position Q10C on the P1 domain did not collide at a detectable rate with the P3−P5 domains of the same subunit, but did exhibit rapid intersubunit collisions. Of the 17 asymmetric, intersubunit collisions analyzed, 11 yielded greater than 50% dimer formation in the mild oxidation reaction, compared with only 1 of 33 symmetric intersubunit disulfides tested under these same conditions (Table 2, Figure 3C). Thus, the asymmetric intersubunit collisions are significantly more rapid than the symmetric intersubunit collisions. The fact that rapid intersubunit collisions, but no intrasubunit collisions, were detected has important implications for the mechanism of the CheA autokinase reaction. To rigorously interpret these findings, however, it is first necessary to assign the multiple products, then determine whether the major products are formed by intra- or interdimer mechanisms.

Assignment of Multiple Products and Discrimination of Intra- versus Interdimer Mechanisms. For each dicysteine mutant, the mild oxidation reaction yielded multiple dimeric products, typically one or two major products and other minor products. In each case, the products were identified by a combination of three complementary approaches: SDS−PAGE migration analysis, subunit exchange analysis, and kinetic analysis (*27*−*32, 38, 39*).

In SDS−PAGE migration analysis, the different dimeric oxidation products for the dicysteine mutant X/Y are resolved by their different migration rates and often can be assigned by comparison with the appropriate migration standards (*32, 38, 39*): (i) The dimeric product containing one symmetric, intersubunit disulfide (X−X′ or Y−Y′) exhibits the same migration rate as the covalent dimer formed from oxidation of the corresponding single-cysteine mutant (Figure 5A, right panel). (ii) The dimeric product containing one intersubunit asymmetric disulfide (X−Y′) typically yields a migration rate intermediate to those of the symmetric dimers X−X′ and Y−Y′ (Figure 5A, right panel). (iii) Covalent dimers formed by dicysteine mutants can contain either one or two intersubunit disulfide bonds. In the latter case, the two disulfides can either be both symmetric (X−X′ and Y−Y′) or both asymmetric (X−Y′ and X′−Y). Such double-disulfide dimers are more compact and migrate more rapidly than single-disulfide dimers, yielding a migration rate between that of monomers and single-disulfide dimers (Figure 5A, right panel).

Subunit exchange analysis provides direct, unambiguous assignment of dimeric products containing a single asymmetric disulfide bond (X−Y′) (*32, 38, 39*). Here the two corresponding single-cysteine mutants (X and Y) are mixed and incubated for 2 h to allow subunit exchange between dimers. The resulting mixed population contains both homo- and heterodimers formed from the two single-cysteine subunits (X,X; Y,Y; X,Y); thus reaction under mild oxidation conditions typically yields three types of covalent dimers (X−X′, Y−Y′, and X−Y′). The migration of the single-cysteine covalent heterodimer (X−Y′) is indistinguishable from the corresponding dicysteine covalent heterodimer containing a single, asymmetric disulfide bond between the same two cysteine positions (X−Y′), allowing direct assignment of the latter. In a representative example (Q10C/S351C), the heterodimer and single asymmetric disulfide-liked dimer (Q10C−S351C′) migrate at identical positions between the two homodimers (Q10C−Q10C′ and S351C−S351C′, Figure 5A, right panel).

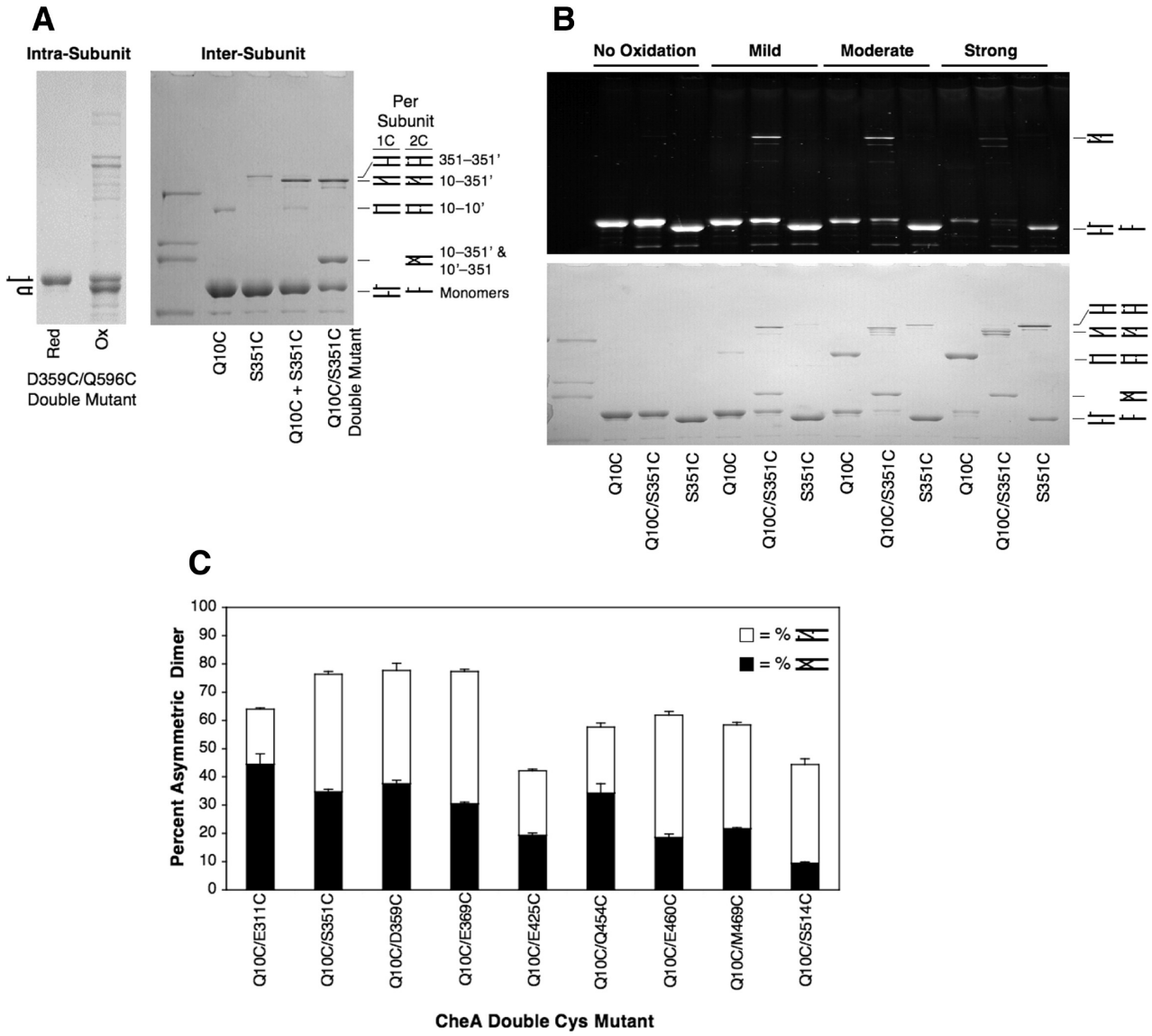

FIGURE 5: Disulfide trapping analysis of asymmetric domain−domain collisions, illustrating three methods to resolve multiple products. (A) In the left panel, SDS−PAGE migration analysis directly assigns intrasubunit disulfide bonds (*28, 32, 39*). Such disulfides make the SDS-denatured polypeptide chain more compact, yielding faster migration than the reduced monomer. In the right panel, SDS−PAGE migration analysis directly assigns symmetric disulfide-linked dimers; for example, comparison of the oxidation products for the single- and double-cysteine mutants Q10C and Q10C/S351C, respectively, indicates that the Q10C−Q10C′ symmetric dimer is a product of both reactions (*31, 32, 38, 39*). Subunit exchange analysis directly identifies some asymmetric disulfide-linked dimers; for example, when the Q10C and S351C homodimers are mixed and incubated for 2 h, subunit exchange forms the Q10C−S351C heterodimer (*31, 32, 38, 39*). Oxidation then reveals a new product, the Q10C−S351C′ disulfide-linked dimer, that is not observed in either of the pure homodimer reactions but migrates between those two symmetric disulfide-linked products. This same product is observed upon oxidation of the dicysteine mutant Q10C/S351C, indicating that the same Q10C−S351C′ intersubunit disulfide bond is formed. Reaction conditions: mild oxidation (see Figure 3 legend). (B) Kinetic analysis directly identifies some products and reveals the time course of product appearance (*38*). Oxidation reactions are quenched by excess 5-fluorescein maleimide (5FM) in SDS, thereby alkylating any remaining free cysteine residues to generate a fluorescent product that is easily detected following SDS−PAGE (upper panel) prior to Coomassie stain analysis (lower panel). In each panel, the Q10C/S351C dicysteine mutant and the corresponding two single-cysteine mutants are subjected to mild, moderate, and strong oxidation conditions, driving the reaction incrementally toward completion. The upper fluorescent product of Q10C/S351C oxidation that appears rapidly during mild oxidation is the asymmetric Q10C−S351C′ single-disulfide dimer, since it migrates between the symmetric Q10C−Q10C′ and S351−S351C′ products and possesses free cysteine residues that react with 5FM. Under strong oxidation conditions, this Q10C−S351C′ single-disulfide product is converted almost completely to the corresponding nonfluorescent, double-disulfide product, which due to its compactness migrates almost as rapidly as monomer and possesses no free cysteine residues to react with 5FM. Reaction conditions: mild oxidation (see Figure 3 legend and Materials and Methods for 5FM reaction). (C) Fraction of CheA converted to asymmetric, single- and double-disulfide products. Of the 17 dicysteine mutants tested (Table 2), these nine dicysteine mutants were found to rapidly form asymmetric, intersubunit disulfide bonds. Further product analysis revealed the fraction of CheA converted to covalent dimers containing one (open) or two (filled) asymmetric disulfide bonds. Reaction conditions: mild oxidation (see Figure 3 legend).

Kinetic analysis of disulfide formation provides additional information that complements the assignments gleaned from SDS−PAGE migration and subunit exchange (*38*). This approach analyzes the order of appearance of products and resolves products containing one or two disulfide bonds by the reaction of free cysteine residues with the cysteine-specific fluorophore 5-fluorescein-maleimide (5FM). The approach subjects a representative dicysteine mutant and its two corresponding single cysteine mutants to mild, moderate, and strong oxidation conditions, then quenches oxidation by

reaction with excess 5FM in SDS, and analyzes the products by both fluorescence imaging and Coomassie staining. In a representative example (Q10C/S351C), the results reveal that the asymmetric single-disulfide product (Q10C−S351C′) forms early and thus is readily apparent in the mild reaction (Figure 5B). This product is assigned by its migration intermediate to the two corresponding symmetric single-disulfide products formed by single-cysteine mutants (Q10C−Q10C′ and S351C−S351C′) and by its labeling with 5FM due to two free cysteine residues. Strikingly, under mild oxidation conditions a dimeric product containing two disulfides also appears and is easily assigned both by its faster migration than the single-disulfide products and by its lack of 5FM labeling indicating that all four cysteine residues of the dimer participate in disulfide bonds (Figure 5B). Because the asymmetric disulfide (Q10C−S351C′) forms much more rapidly than either symmetric disulfide under mild conditions (Figure 5B), it follows that the double-disulfide product contains two asymmetric bonds (Q10C−S351C′/Q10C′−S351C). As the reaction proceeds the asymmetric single-disulfide product eventually disappears as indicated by the loss of the upper, fluorescent band (Figure 5B), while the asymmetric double-disulfide product builds up with time, as indicated by the increasing ratio of this product to unreacted monomer (Figure 5B). Overall, the results indicate that the asymmetric single-disulfide product is rapidly formed and converted to the asymmetric double-disulfide product as the reaction proceeds.

Using all three assignment strategies, we identified the major products formed by each of the 17 dicysteine mutants under mild oxidation conditions. As noted above, all 17 dicysteine mutants yielded disulfide-linked dimers. Altogether, of the 11 mutants that rapidly formed dimers, nine yielded primarily asymmetric products (Table 2). Further product analysis of these nine reactions revealed the relative contributions of asymmetric single- and double-disulfide products (Figure 5C). Finally, to resolve intra- and interdimer collision mechanisms, the CheA concentration dependence of the dimer formation rate was determined for the nine rapid asymmetric disulfide formers as described above for symmetric disulfide products. Of these nine reactions, eight were dominated ($\geq$80%) by the intradimer collisional mechanism. The remaining reaction exhibited a larger component of interdimer collisions (51% $\pm$ 5%), which caused the appearance of higher order covalent oligomers in SDS−PAGE representing chains of three or more subunits linked by interdimer disulfides (data not shown).

Thus, mild oxidation of the 17 dicysteine mutants enabled the detection of eight rapidly forming asymmetric disulfide bonds arising from collisions between the P1 domain and a different domain in the sister subunit. These eight rapid, asymmetric disulfide reactions were all significantly faster than the seven fastest symmetric reactions observed for single-cysteine mutants. Of the eight rapid asymmetric collisions, all but one were between P1 and P4′, the substrate and catalytic domains of the adjacent subunits. In stark contrast, no collisions were detected between P1 and other domains of the same subunit. Overall, the findings indicate that the P1 substrate domain is constrained to collide primarily with the P4′ catalytic domain of its sister subunit in the same CheA dimer, thereby providing a direct motional explanation for the known, trans-subunit phosphorylation mechanism of CheA autophosphorylation.

At first glance, the observation of seven rapid asymmetric collisions between P1 and P4′, in each case yielding significant fractions of double-disulfide product, may appear to contradict the published observation that CheA exhibits negative cooperativity such that kinase activity is dominated by only one of the two P1−P4′ interactions possible in the dimer at any point in time (*45*). Actually, however, the formation of P1−P4′ double-disulfide products is fully compatible with such negative cooperativity. For example, the P1−P4′ disulfide bond could form first between a proximal cysteine pair in the "active" P1−P4′ domain pair. Subsequently, the P1′−P4 disulfide could form between a more distal cysteine pair in the "inactive" P1′−P4 domain pair. The latter collision may require a relative domain motion that strays away from the lowest energy conformation of the CheA dimer, but such a motion could in principle be generated by simple thermal domain motions.

DISCUSSION

Mapping out the Spatial Ranges and Kinetics of CheA Domain Motions. Figure 6A,B summarizes the seven symmetric and eight asymmetric cysteine pairs, respectively, that detect the 15 most rapid collisions between the two sister subunits in the apo-CheA dimer via disulfide bond formation. Each of these cysteine pairs is functional and retains CheA autokinase activity in the reduced state. Both sets of data indicate that the P1 substrate domain is highly mobile at the end of its long, flexible tether, since four of the seven rapid symmetric reactions trap P1−P1′ collisions (Figure 6A) and all eight of the rapid asymmetric reactions trap collisions between P1 and P4′ (seven examples) or P3′ (one example) (Figure 6B). Notably, no collisions are trapped between P1 and the P3−P5 domains of the same subunit nor between P1 and the P5′ domain of the sister subunit. The seven rapid P1−P4′ collisions and the rapid P1−P3′ collision are detected easily under mild oxidation conditions are significantly faster than the four fastest P1−P1′ collisions detected under moderate oxidation conditions. It follows that the tethered P1 substrate domain spends most of its time moving within a defined region of space, the region surrounding the P4′ catalytic domain of the sister subunit.

Although the main focus of the present study is the mobility of the P1 domain, more limited information is provided about the motions of the P2, P4, and P5 domains from the analysis of symmetric cysteine pairs. Figure 6A shows that for each of these domains, a single cysteine pair detects symmetric collisions between the two corresponding domains of the dimer. These collisions are slower than the rapid P1−P4′ collisions, but are easily detected under moderate oxidation conditions. Most surprising are the large amplitudes of the observed P4−P4′ and P5−P5′ collisions. Unlike the P1 domain, these domains are not coupled to their adjacent domains via long flexible tethers. Modest P3−P5 domain mobility arising from interdomain hinges has been observed in previous structural studies (*15, 23*), but the disulfide trapping approach reveals that such motions possess surprisingly large amplitudes. The "open-winged butterfly" configuration of the P3−P5 core is likely one of the conformations sampled by the dynamic CheA dimer in

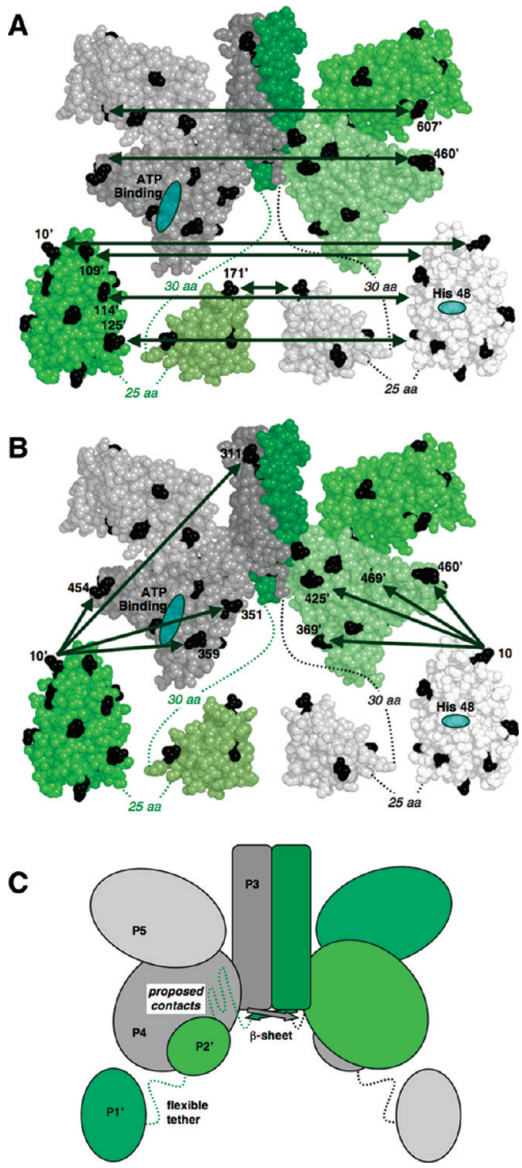

FIGURE 6: Schematic depiction of rapid domain−domain collisions detected by disulfide trapping, and a working model for the constrained mobility of the P1 substrate domain. (A) The seven most rapid symmetric domain−domain collisions observed in the CheA homodimer. These intradimer collisions yield the formation of disulfide bonds between the pairs of symmetric cysteine residues connected by the arrow. (B) The eight most rapid asymmetric domain−domain collisions observed in the CheA homodimer. These intradimer collisions yield disulfide bonds between (i) the probe Q10C residue on the P1 substrate domain and (ii) a second cysteine residue on a different domain of the sister subunit, as indicated by the arrows. The collisions indicated in panels A and B all occur on the millisecond time scale or faster at 30 °C, and the asymmetric collisions are faster than the symmetric collisions. (C) Working model for constraints on the mobility of the P1 substrate domain. Constraints are needed to explain the observation that P1 collides most rapidly with positions on the surface of its target domain, the P4′ catalytic domain of the sister (trans) subunit, while no collisions between P1 and other domains of its own (cis) subunit are detected. The model hypothesizes that the intersubunit antiparallel β-sheet at the N-terminus of the four-helix P3−P3′ dimerization motif directs the P2−P3 linker away from the cis subunit and toward the trans subunit as previously proposed (*15*). In addition, the P2−P3 linker or the P2 domain is hypothesized to associate with unknown sites on the trans subunit, thereby anchoring the P1−P2 linker and the P1 domain in the vicinity of the trans-P4′ domain. Such a model explains the known trans-autophosphorylation mechanism of CheA kinase.

solution. Assuming this state as the starting conformation (Figure 6A), each of the P4−P4′ and P5−P5′ collisions would require tilting the wings to the closed position, which would bring the relevant cysteine pair into proximity. It appears likely, however, that in this closed conformation additional domain rotations, or local backbone motions, would be also required for disulfide bond formation. In short, as is often the case in multidomain proteins (*29, 42, 43*), the domains of CheA undergo large amplitude relative thermal motions in solution.

Alternatively, one could propose that the observed large-amplitude P4−P4′ and P5−P5′ collisions occur during events in which the P3−P3′ dimerization motif dissociates to allow free rotation of the two subunits relative to each other. However, such dissociation events are likely to be too slow to account for the observed disulfide formation rates, since the four-helix bundle formed by the two P3 domains is both thermodynamically and kinetically stable (*15, 21*). The bundle is stabilized by hydrophobic contacts spanning an area of 2000 Å^2 on the surface of each P3 helical hairpin, generating a large free energy barrier to dissociation. At the temperature of the current study (30 °C), the dimer dissociation rate is slow ($k = 0.008$ s^{-1} for the highly homologous *E. coli* CheA dimer) (*15, 21*). It follows that the half-life of the dimer (over 1 min) is significantly longer than the rapid intradimer disulfide formation reactions observed herein (half-lives all under 1 min). Furthermore, only a small fraction of individual dissociation events would be expected to yield disulfide bond formation since the present oxidation conditions convert an exceeding small fraction of cysteine−cysteine collisions to disulfide bonds (*28*, see below). Thus, it is likely that the 15 most rapidly formed disulfides are generated by domain−domain collisions within the stable dimer.

The observed rates of symmetric and asymmetric disulfide bond formation place a lower limit on the frequencies of the observed collisions. To a first approximation, for surface-exposed cysteine residues, the rate of disulfide formation (R_{S-S}, rate constant k_{S-S}) is directly proportional to the sulfhydryl−sulfhydryl collision rate (R_c, rate constant k_c):

$$R_{S-S} = R_c\sigma \quad \text{or} \quad k_{S-S} = k_c\sigma \tag{1}$$

where the efficiency factor of disulfide formation (σ) is a proportionality constant representing the fraction of collisions that are successfully converted to disulfide bonds. Typically the efficiency factor is much less than unity (*28*). For the moderate oxidation system, the efficiency factor is $\sigma \leq 2 \times 10^{-5}$ (extrapolated to the current pH of 7.5, where σ is too fast to measure, from σ measurements at lower pH values; see ref *28*), indicating that over 50,000 collisions are needed to form a disulfide bond. The 15 most rapid symmetric and asymmetric disulfide formation reactions (Figures 6A,B) are all intramolecular and possess half-lives under 1 min when driven by moderate oxidation conditions, corresponding to intramolecular disulfide formation rate constants of $k_{S-S} \geq 0.012$ s^{-1} molecule^{-1}. Equation 1 transforms these disulfide formation rate constants into collisional rate constants of $k_c \geq 10^3$ s^{-1} molecule^{-1}. Thus, in a given dimer, each of these collisions occurs on a millisecond time scale or faster and is quite rapid compared with the free kinase turnover rate of $k_{cat} \approx 0.03-0.2$ s^{-1} molecule^{-1} (*12, 26*).

Implications for CheA Function. All of the CheA kinase active site residues are located on the P1 substrate and P4 catalytic domains (*15, 18*). The normal CheA autokinase reaction is known to be a trans reaction in which the catalytic ATP binding site on the P4 domain of one subunit phosphorylates the His48′ side chain on the P1′ domain of the other subunit in the same dimer (*12, 13, 26*). Thus, the spatial range of the P1 substrate domain observed herein, where P1 is constrained to collide primarily with the P4′ catalytic domain of its sister subunit (Figure 6B), fully explains the trans mechanism of the CheA autokinase reaction. These spatial constraints on P1 movements ensure that it rarely collides with the catalytic domain of the same subunit, thereby making the rate of cis-autophosphorylation negligible. The slower P1−P1′ collisions detected herein also have important functional implications, since it is known that in CheA-short the two truncated P1 domains associate to increase the stability of the homodimer (*37*). Finally, the hinge motions of the type that allow P4−P4′ and P5−P5′ collisions (Figure 6A) may well be important to the docking interactions of CheA during assembly of the receptor−CheA−CheW signaling complex (*24*).

While these initial studies have focused on free apo-CheA in solution, the constrained mobility of the P1 domain observed herein provides a potential mechanism of kinase regulation in the assembled receptor−CheA−CheW signaling array. In principle, while the present study shows that P1 domain motions are rapid compared with the k_{cat} of free CheA, these P1 motions could become rate-limiting in the assembled signaling complex if the motions are slower or k_{cat} is faster. In this case, the on-state of the receptor could stimulate CheA autophosphorylation rate by sterically "focusing" the collisions of the P1 domain with the catalytic site on P4′. Or the off-state of the receptor could bind the P1 domain or sterically hinder its collision with the catalytic site. Future disulfide trapping studies of P1 domain motions in the complex of CheA with substrate ATP or with a nonhydrolyzable ATP analogue, as well as in the assembled signaling array, are needed to test these and other possibilities.

Working Model for the Constrained Dynamics of the P1 Substrate Domain. As Figure 1A illustrates, the long P1−P2 and P2−P3 linkers would, in the absence of any constraints, allow collision of P1 substrate domain with all surfaces of both CheA subunits. However, the available evidence indicates that constraints must exist since P1 does not collide with all surfaces but instead is found to be located primarily in the vicinity of the P4′ catalytic domain and since P1 phosphorylation by a cis mechanism is negligible. Moreover, the results suggest that these constraints cause the surface of the P1 domain containing the probe Q10C cysteine to collide most rapidly with the surface of the P4 domain containing S351C, D359C, and E369C (Figure 5C). While the present findings do not define the nature of the constraints, it is clear that the constraints on P1 mobility are crucial to the trans mechanism of autophosphorylation and may also serve to prevent the N-terminal polypeptide chains of the two subunits from wrapping around each other to become intertwined (Figure 1).

One constraint capable of modulating the average location of P1 is its docking to the P4′ catalytic domain. Two P1 docking modes have been proposed (*15, 24, 44*): docking to the ATP binding site as required for the autokinase reaction and docking to a second site on the P4 domain that may inhibit autophosphorylation. Such docking would bias the distribution of sampled locations, thereby increasing the probability that P1 would remain proximal to the catalytic domain. However, since a given P1 domain could, in principle, bind with equal affinity to either of the two identical catalytic domains, P4 and P4′, in the same dimer, such buffered diffusion cannot explain the observed propensity for P1 to collide with only the P4′ domain on the sister subunit (Figure 6B) and to be phosphorylated only by a trans-autokinase mechanism.

Instead, the initial working model of Figure 6C proposes other types of constraints that would specifically restrict P1 to the vicinity of P4′. It is known from crystal structures of the P3−P5 core that the N-terminal regions of P3 and P3′ form an antiparallel β-sheet that directs each P2−P3 linker toward the opposite subunit (*15*). The working model proposes that the P2−P3 linker, and perhaps the P2 domain as well, bind to the trans subunit or are otherwise sterically constrained by the trans subunit, thereby limiting the freedom of P1 motion to that allowed by the P1−P2 linker. More broadly, since most CheAs share long linkers of variable lengths, analogous mobility constraints are likely to be a widespread feature of this large class of bacterial kinases, thereby maximizing the efficiency of their trans-autophosphorylation reactions.

ACKNOWLEDGMENT

The authors gratefully acknowledge Profs. Howard Berg, John S. Parkinson, and Victor Sourjik for gifts of plasmids and strains; Drs. Aaron S. Miller and Susan Kohout for construction of single-cysteine CheA mutants; Dr. Joshua Bornhorst for construction of cysteine-less CheA; Susanne Buehler for technical advice and assay development; and members of the Falke laboratory (Dr. Jeff Knight, Dr. Annette Erbse, Kyle Landgraf, and Ka Lin Swain) for helpful comments on the manuscript. Finally, thanks to Drs. Brian Crane, Michael Manson, and John S. Parkinson for helpful discussions during the development of the project.

REFERENCES

1. Hazelbauer, G. L., Falke, J. J., and Parkinson, J. S. (2008) Bacterial chemoreceptors: High-performance signaling in networked arrays. *Trends Biochem. Sci. 33*, 9–19.
2. Baker, M. D., Wolanin, P. M., and Stock, J. B. (2006) Signal transduction in bacterial chemotaxis. *Bioessays 28*, 9–22.
3. Wadhams, G. H., and Armitage, J. P. (2004) Making sense of it all: Bacterial chemotaxis. *Nat. Rev. Mol. Cell. Biol. 5*, 1024–1037.
4. Stock, J. B., Levit, M. N., and Wolanin, P. M. (2002) Information processing in bacterial chemotaxis. *Sci. STKE 2002*, PE25.
5. Stock, A. M., Robinson, V. L., and Goudreau, P. N. (2000) Two-component signal transduction. *Annu. Rev. Biochem. 69*, 183–215.
6. Falke, J. J., Bass, R. B., Butler, S. L., Chervitz, S. A., and Danielson, M. A. (1997) The two-component signaling pathway of bacterial chemotaxis: a molecular view of signal transduction by receptors, kinases, and adaptation enzymes. *Annu. Rev. Cell Dev. Biol. 13*, 457–512.
7. Khursigara, C. M., Wu, X., and Subramaniam, S. (2008) Chemoreceptors in *Caulobacter crescentus*: Trimers of receptor dimers in a partially ordered hexagonally packed array. *J. Bacteriol. 190*, 6805–6810.
8. Briegel, A., Ding, H. J., Li, Z., Werner, J., Gitai, Z., Dias, D. P., Jensen, R. B., and Jensen, G. J. (2008) Location and architecture of the *Caulobacter crescentus* chemoreceptor array. *Mol. Microbiol. 69*, 30–41.

9. Kentner, D., and Sourjik, V. (2006) Spatial organization of the bacterial chemotaxis system. *Curr. Opin. Microbiol. 9*, 619–624.
10. Maddock, J. R., and Shapiro, L. (1993) Polar location of the chemoreceptor complex in the *Escherichia coli* cell. *Science 259*, 1717–1723.
11. Erbse, A. H., and Falke, J. J. (2009) The core signaling proteins of bacterial chemotaxis assemble to form an ultrastable complex, *Biochemistry*, submitted for publication.
12. Surette, M. G., Levit, M., Liu, Y., Lukat, G., Ninfa, E. G., Ninfa, A., and Stock, J. B. (1996) Dimerization is required for the activity of the protein histidine kinase CheA that mediates signal transduction in bacterial chemotaxis. *J. Biol. Chem. 271*, 939–945.
13. Swanson, R. V., Bourret, R. B., and Simon, M. I. (1993) Intermolecular complementation of the kinase activity of CheA. *Mol. Microbiol. 8*, 435–441.
14. Jahreis, K., Morrison, T. B., Garzon, A., and Parkinson, J. S. (2004) Chemotactic signaling by an *Escherichia coli* CheA mutant that lacks the binding domain for phosphoacceptor partners. *J. Bacteriol. 186*, 2664–2672.
15. Bilwes, A. M., Alex, L. A., Crane, B. R., and Simon, M. I. (1999) Structure of CheA, a signal-transducing histidine kinase. *Cell 96*, 131–141.
16. Morrison, T. B., and Parkinson, J. S. (1994) Liberation of an interaction domain from the phosphotransfer region of CheA, a signaling kinase of *Escherichia coli*. *Proc. Natl. Acad. Sci. U.S.A. 91*, 5485–5489.
17. Mourey, L., Da Re, S., Pedelacq, J. D., Tolstykh, T., Faurie, C., Guillet, V., Stock, J. B., and Samama, J. P. (2001) Crystal structure of the CheA histidine phosphotransfer domain that mediates response regulator phosphorylation in bacterial chemotaxis. *J. Biol. Chem. 276*, 31074–31082.
18. Quezada, C. M., Hamel, D. J., Gradinaru, C., Bilwes, A. M., Dahlquist, F. W., Crane, B. R., and Simon, M. I. (2005) Structural and chemical requirements for histidine phosphorylation by the chemotaxis kinase CheA. *J. Biol. Chem. 280*, 30581–30585.
19. Stewart, R. C., Jahreis, K., and Parkinson, J. S. (2000) Rapid phosphotransfer to CheY from a CheA protein lacking the CheY-binding domain. *Biochemistry 39*, 13157–13165.
20. McEvoy, M. M., Muhandiram, D. R., Kay, L. E., and Dahlquist, F. W. (1996) Structure and dynamics of a CheY-binding domain of the chemotaxis kinase CheA determined by nuclear magnetic resonance spectroscopy. *Biochemistry 35*, 5633–5640.
21. Park, S. Y., Quezada, C. M., Bilwes, A. M., and Crane, B. R. (2004) Subunit exchange by CheA histidine kinases from the mesophile Escherichia coli and the thermophile *Thermotoga maritima*. *Biochemistry 43*, 2228–2240.
22. Zhao, J., and Parkinson, J. S. (2006) Mutational analysis of the chemoreceptor-coupling domain of the *Escherichia coli* chemotaxis signaling kinase CheA. *J. Bacteriol. 188*, 3299–3307.
23. Park, S. Y., Borbat, P. P., Gonzalez-Bonet, G., Bhatnagar, J., Pollard, A. M., Freed, J. H., Bilwes, A. M., and Crane, B. R. (2006) Reconstruction of the chemotaxis receptor-kinase assembly. *Nat. Struct. Mol. Biol. 13*, 400–407.
24. Miller, A. S., Kohout, S. C., Gilman, K. A., and Falke, J. J. (2006) CheA Kinase of bacterial chemotaxis: Chemical mapping of four essential docking sites. *Biochemistry 45*, 8699–8711.
25. Zhou, H., McEvoy, M. M., Lowry, D. F., Swanson, R. V., Simon, M. I., and Dahlquist, F. W. (1996) Phosphotransfer and CheY-binding domains of the histidine autokinase CheA are joined by a flexible linker. *Biochemistry 35*, 433–443.
26. Hess, J. F., Bourret, R. B., and Simon, M. I. (1988) Histidine phosphorylation and phosphoryl group transfer in bacterial chemotaxis. *Nature 336*, 139–143.
27. Falke, J. J., and Koshland, D. E., Jr. (1987) Global flexibility in a sensory receptor: a site-directed cross-linking approach. *Science 237*, 1596–1600.
28. Careaga, C. L., and Falke, J. J. (1992) Thermal motions of surface alpha-helices in the D-galactose chemosensory receptor. Detection by disulfide trapping. *J. Mol. Biol. 226*, 1219–1235.
29. Careaga, C. L., Sutherland, J., Sabeti, J., and Falke, J. J. (1995) Large amplitude twisting motions of an interdomain hinge: a disulfide trapping study of the galactose-glucose binding protein. *Biochemistry 34*, 3048–3055.
30. Butler, S. L., and Falke, J. J. (1996) Effects of protein stabilizing agents on thermal backbone motions: A disulfide trapping study. *Biochemistry 35*, 10595–10600.
31. Bass, R. B., and Falke, J. J. (1999) The aspartate receptor cytoplasmic domain: In situ chemical analysis of structure, mechanism and dynamics. *Structure 7*, 829–840.
32. Bass, R. B., Butler, S. L., Chervitz, S. A., Gloor, S. L., and Falke, J. J. (2007) Use of site-directed cysteine and disulfide chemistry to probe protein structure and dynamics: Applications to soluble and transmembrane receptors of bacterial chemotaxis. *Methods Enzymol. 423*, 25–51.
33. Bornhorst, J. A., and Falke, J. J. (2000) Purification of proteins using polyhistidine affinity tags. *Methods Enzymol. 326*, 245–254.
34. Laemmli, U. K. (1970) *Nature 227*, 680–685.
35. Kohout, S. C., Corbalan-Garcia, S., Gomez-Fernandez, J. C., and Falke, J. J. (2003) C2 domain of protein kinase C alpha: Elucidation of the membrane docking surface by site-directed fluorescence and spin labeling. *Biochemistry 42*, 1254–1265.
36. Tawa, P., and Stewart, R. C. (1994) Kinetics of CheA autophosphorylation and dephosphorylation reactions. *Biochemistry 33*, 7917–7924.
37. Kott, L., Braswell, E. H., Shrout, A. L., and Weis, R. M. (2004) Distributed subunit interactions in CheA contribute to dimer stability: A sedimentation equilibrium study. *Biochim. Biophys. Acta 1696*, 131–140.
38. Swain, K. E., and Falke, J. J. (2007) Structure of the conserved HAMP domain in an intact, membrane-bound chemoreceptor: A disulfide mapping study. *Biochemistry 46*, 13684–13695.
39. Falke, J. J., Dernburg, A. F., Sternberg, D. A., Zalkin, N., Milligan, D. L., and Koshland, D. E., Jr. (1988) Structure of a bacterial sensory receptor. A site-directed sulfhydryl study. *J. Biol. Chem. 263*, 14850–14858.
40. Wang, E. A., Mowry, K. L., Clegg, D. O., and Koshland, D. E., Jr. (1982) Tandem duplication and multiple functions of a receptor gene in bacterial chemotaxis. *J. Biol. Chem. 257*, 4673–4676.
41. Hazelbauer, G. L., Mesibov, R. E., and Adler, J. (1969) *Escherichia coli* mutants defective in chemotaxis toward specific chemicals. *Proc. Natl. Acad. Sci. U.S.A. 64*, 1300–1307.
42. Gerstein, M., Lesk, A. M., and Chothia, C. (1994) Structural mechanisms for domain movements in proteins. *Biochemistry 33*, 6739–6749.
43. Bennett, W. S., and Huber, R. (1984) Structural and functional aspects of domain motions in proteins. *CRC Crit. Rev. Biochem. 15*, 291–384.
44. Hamel, D. J., Zhou, H., Starich, M. R., Byrd, R. A., and Dahlquist, F. W. (2006) Chemical-shift-perturbation mapping of the phosphotransfer and catalytic domain interaction in the histidine autokinase CheA from *Thermotoga maritima*. *Biochemistry 45*, 9509–9517.
45. Levit, M., Liu, Y., Surette, M., and Stock, J. (1996) Active site interference and asymmetric activation in the chemotaxis protein histidine kinase CheA. *J. Biol. Chem. 271*, 32057–32063.

BI900033R